Vervelidou, F., Lesur, V. (2018): Unveiling Earth's Hidden Magnetization. - *Geophysical Research Letters*, *45*, 22, pp. 12,283—12,292.

DOI: http://doi.org/10.1029/2018GL079876

AGU100 ADVANCING EARTH AND SPACE SCIENCE

Geophysical Research Letters

RESEARCH LETTER
10.1029/2018GL079876

Key Points:
- More than half of Earth's magnetization is hidden in the sense that it generates no observable magnetic field signal
- Under few reasonable assumptions, we uniquely recover most of Earth's hidden magnetization from a lithospheric magnetic field model
- Recovering the hidden part of Earth's magnetization enables a better link to the underlying internal processes

Supporting Information:
- Supporting Information S1

Correspondence to:
F. Vervelidou,
foteini@gfz-potsdam.de

Citation:
Vervelidou, F., & Lesur, V. (2018). Unveiling Earth's hidden magnetization. *Geophysical Research Letters*, *45*, 12,283–12,292. https://doi.org/10.1029/2018GL079876

Received 2 AUG 2018
Accepted 9 NOV 2018
Accepted article online 15 NOV 2018
Published online 29 NOV 2018

Unveiling Earth's Hidden Magnetization

Foteini Vervelidou[1] **and Vincent Lesur**[2]

[1]Helmholtz Centre Potsdam-GFZ German Research Centre for Geosciences, Geomagnetism, Potsdam, Germany, [2]Institut de Physique du Globe de Paris, Sorbonne Paris Cité, Université Paris Diderot, UMR 7154 CNRS, Paris, France

Abstract Rock magnetization carries information about rocks' properties, Earth's tectonic history, and evolution of its core magnetic field. One way to study Earth's magnetization is through the magnetic signal it generates, known as the lithospheric magnetic field. Although there exist global lithospheric magnetic field models of high spatial resolution, this path has not yet been very fruitful because of an important limitation: only part of the magnetization is *visible*, that is, produces an observable magnetic field signal. We refer to the remaining part of the magnetization as the *hidden* magnetization, and we recover it from a lithospheric magnetic field model under a few reasonable assumptions. We find that Earth's hidden magnetization at high and middle latitudes is very similar, both in intensity and shape, to Earth's visible magnetization. At low latitudes, the estimated hidden magnetization relies on a priori information and can be very different from the visible one.

Plain Language Summary Earth's uppermost layer is abundant in magnetized rocks. Rocks' magnetization acts as a recorder of many processes taking place inside the Earth, from the crust down to the core, which lies almost 3,000 km far from the surface. Currently, the most common way to extract this information is through laboratory measurements of rock samples. An alternative way is to study the magnetic signal of magnetized rocks, which is known as the lithospheric magnetic field. This is measured by satellites orbiting around the Earth and airborne and marine missions. Inferring, however, the direction and the strength of the magnetization from magnetic field measurements is not straightforward. The reason is that a large part of a given magnetization generates no magnetic field. We call this part of the magnetization *hidden* as opposed to the remaining part, which we call *visible*. In this study, we show how the visible and the hidden parts of the magnetization are linked to each other. This link allows us to uniquely recover most of Earth's hidden magnetization. Recovering this part of Earth's magnetization enables a better link to the underlying processes, like crustal thickness contrasts, temperature gradients, hydrothermal activity, or deposits of highly magnetic minerals like magnetite.

1. Introduction

The upper part of the Earth's lithosphere is abundant in ferromagnetic minerals, at least down to the seismic Moho discontinuity (Vervelidou & Thébault, 2015; Wasilewski et al., 1979) and in some places probably even deeper (Ferré et al., 2014). Below their Curie temperature, these minerals have high magnetic susceptibility. Therefore, their magnetic moments tend to align along the direction of Earth's magnetic field, which is mainly generated in Earth's outer core. The bulk magnetic moment per unit volume that is generated through this alignment is known as the induced magnetization. It is proportional to the inducing magnetic field, with the magnetic susceptibility being the proportionality factor. Induced magnetization is the source of a secondary magnetic field, known as the induced lithospheric magnetic field. Ferromagnetic minerals have the additional property of being able to retain remanent magnetization. Remanent magnetization is *frozen in* the rocks as they cool below their Curie temperature and remains present even after the removal of the inducing magnetic field. It is this property of rocks that makes them a valuable record of the past magnetic field and also of tectonic motions and true polar wander (Besse & Courtillot, 2002; Vine & Matthews, 1963).

It is long known that only part of the rocks' magnetization, whether of induced or remanent origin, contributes to the lithospheric magnetic field (Jackson et al., 1999; Lesur & Jackson, 2000; Maus & Haak, 2003; Runcorn, 1975). This limits severely our ability to use the lithospheric magnetic field as a source of information for the study of solid Earth since several distributions of magnetized material can generate the same magnetic field.

Efforts to tackle this nonuniqueness include solving for the minimum norm solution (Parker, 2003; Whaler & Langel, 1996) or a part of the solution (Arkani-Hamed & Strangway, 1985), imposing constraints on the underlying source's geometry (e.g., Quesnel et al., 2009) and forward modeling based on geological, tectonic, and age considerations (Dyment et al., 2015; Hemant & Maus, 2005; Masterton et al., 2013). An alternative approach that has been used both in forward calculations and inverse problems is the technique of equivalent dipoles (e.g., Fox Maule et al., 2005; Purucker et al., 1998). Although this technique allows modeling the entire magnetization, it is based on a priori concerning the depth and lateral distribution of dipoles. This a priori affects the solution strongly because the basis functions, that is, the dipoles, are of infinite spectral content as opposed to the magnetic field data. Moreover, the mathematical framework of this technique does not allow to separate the part of the magnetization that can be uniquely recovered from the magnetic field data from the part that requires independent a priori information.

It was not until the introduction of vector spherical harmonics in the study of Earth's magnetization (Gubbins et al., 2011) that the part of the magnetization that does not contribute to the observable magnetic field, hereafter called the hidden magnetization, could be studied separately from its contributing part: the visible magnetization. This decomposition partially alleviated the nonuniqueness since for a magnetized layer of given thickness, the visible magnetization of a given lithospheric magnetic field is unique. Any set of lithospheric magnetic field Spherical Harmonic (SH) coefficients can, therefore, be converted to a set of visible magnetization vector SH coefficients (Gubbins et al., 2011). The latter, in the case of induced magnetization, can be related to the SH coefficients of the magnetic susceptibility and the SH coefficients of the inducing magnetic field (Vervelidou, Lesur, Grott, et al., 2017). Similarly, expressions that relate the magnetic susceptibility and the inducing field to the hidden part of the magnetization can be established. For this, the hidden magnetization has to be decomposed in toroidal and poloidal parts (see section 3). Overall, three expressions, taken together, relate the total magnetization to the magnetic susceptibility for a given inducing magnetic field. We use them to infer the total magnetization from a lithospheric magnetic field model. In particular, we first infer the susceptibility from the visible magnetization, by solving an inverse problem, and then we use the susceptibility to estimate the hidden magnetization. Under the assumption of a magnetized layer of constant thickness carrying only induced magnetization that varies laterally, we show that most of the hidden magnetization can be uniquely recovered. Moreover, we characterize entirely the part of the hidden magnetization that remains inaccessible from magnetic field data, for the case of a dipolar inducing magnetic field (see the supporting information). For this part of the hidden magnetization to be recovered, a priori information is required.

2. Data

Our input lithospheric magnetic field model has been derived from satellite and airborne and marine magnetic field measurements. In particular, for spatial scales down to 450 km (SH degrees 16 to 90), we used the Dedicated Lithospheric Field Model (Thébault et al., 2016), a product of the European Space Agency (ESA) Swarm multisatellite mission (Friis-Christensen et al., 2006). This model is derived from measurements acquired by satellites Alpha and Charlie, the lower Swarm satellites flying side by side. For shorter spatial scales, down to 200 km (SH degrees 91 to 200), we used the SH model obtained from the second version of the World Digital Magnetic Anomaly Map (WDMAM; Khorhonen et al., 2007; Lesur et al., 2016). WDMAM is a global compilation of airborne and marine lithospheric magnetic field data, continuously updated in the framework of an international scientific project, which runs under the auspices of International Association of Geomagnetism and Aeronomy (IAGA) and Commission for the Geological Map of the World (wdmam.org).

For these spatial scales, the assumption of the magnetization being entirely induced is a realistic one, particularly over the continents. First, remanent magnetization aligned with the present-day core magnetic field direction cannot be distinguished from induced magnetization. Second, the magnetic effect of remanent magnetization averages out over large spatial scales due to the polarity reversals of Earth's core magnetic field over geological times (e.g., Arkani-Hamed & Strangway, 1985). Notable exceptions over the oceanic region include the Cretaceous quiet zones. According to the oceanic magnetization model by Masterton et al. (2013), estimated up to SH degree 256, remanence contributes 24% to the energy of the total oceanic magnetization. They note, however, that their model might underestimate the actual contribution of remanence. In this respect, our results over the oceanic region should be interpreted with caution. Spatial scales corresponding

to SH degrees 1–16 of the lithospheric magnetic field remain unknown as they are concealed by the Earth's core magnetic field (Thébault et al., 2010).

To recover the part of the hidden magnetization that cannot be retrieved from magnetic field data, we used the Vertically Integrated Susceptibility (VIS) model by Hemant and Maus (2005). This model assigns magnetic susceptibility values to different regions of the Earth, based on the region's geological province, age, petrology, and stratigraphic thickness, according to available geologic, tectonic, and seismic thickness maps; drilling studies; and magnetic susceptibility catalogs based on laboratory measurements. Over some regions, the model has been subsequently revisited to account better for the magnetic field model MF3, derived from CHAllenging Minisatellite Payload (CHAMP) satellite magnetic field measurements (Maus et al., 2006).

3. Methods

3.1. From the Lithospheric Magnetic Field to the Visible Magnetization

The lithospheric magnetic field at point **r** is commonly expressed as a series of SH

$$\mathbf{B}_{\text{lith}}(\mathbf{r}) = -\nabla\left(R\sum_{l}\sum_{m=-l}^{l} g_l^m Y_l^m(\theta,\phi)\left(\frac{R}{r}\right)^{l+1}\right), \tag{1}$$

where Y_l^m are the SH of degree l and order m, g_l^m are the SH coefficients, R is their reference radius, and $\{r,\theta,\phi\}$ the geocentric spherical coordinates of **r**.

Any surface distribution of magnetization $\mathbf{M}(\theta,\phi)$ can be decomposed in three components (Gubbins et al., 2011)

$$\mathbf{M} = \mathcal{I} + \mathcal{E} + \mathcal{T}, \tag{2}$$

with

$$\mathcal{I} = \sum_{l}\sum_{m=-l}^{l} g_{\mathcal{I},l}^m \mathbf{Y}_{l,l-1}^m, \quad \mathcal{E} = \sum_{l}\sum_{m=-l}^{l} g_{\mathcal{E},l}^m \mathbf{Y}_{l,l+1}^m, \quad \mathcal{T} = \sum_{l}\sum_{m=-l}^{l} g_{\mathcal{T},l}^m \mathbf{Y}_{l,l}^m, \tag{3}$$

where $\mathcal{I}$, $\mathcal{E}$, and $\mathcal{T}$ stand for the visible, hidden poloidal, and hidden toroidal magnetization, respectively; $g_{\mathcal{I},l}^m$, $g_{\mathcal{E},l}^m$, and $g_{\mathcal{T},l}^m$ are the respective vector SH coefficients; and $\mathbf{Y}_{l,l-1}^m$, $\mathbf{Y}_{l,l+1}^m$, and $\mathbf{Y}_{l,l}^m$ are the three types of real vector spherical harmonics (see Vervelidou, Lesur, Grott, et al., 2017, their equations 5–7).

Introducing the above expressions into the known relation (see, eg., Blakely, 1996) linking the magnetization, **M**, to the magnetic field it generates, $\mathbf{B}_{\text{lith}}$, allows to derive an expression linking the SH coefficients of the visible magnetization to the SH coefficients of the lithospheric magnetic field (Gubbins et al., 2011, for an infinitesimally thin magnetized layer). For a magnetized layer of finite thickness, Vervelidou, Lesur, Grott, et al. (2017) obtained the following expression (see their equation 11)

$$g_{\mathcal{I},l}^m = \frac{l+2}{\mu_0}\sqrt{\frac{2l+1}{l}}\frac{1}{\left[1-\left(1-\frac{t}{R}\right)^{l+2}\right]} g_l^m, \tag{4}$$

where $g_{\mathcal{I},l}^m$ are given in units of nanoampere per meter (nA/m), g_l^m in units of nanotesla (nT), the reference radius R is also the radius of the upper spherical surface of the magnetized layer, t is the thickness of the magnetized layer and μ_0 is the magnetic permeability of empty space.

Here using the above equation, we converted the input lithospheric field model to a visible magnetization model ($\mathcal{I}_{\text{input}}$ in Figure 1, which summarizes the workflow of our study schematically), under the assumption of a 30-km-thick magnetized layer (as estimated in Thébault & Vervelidou, 2015). We note that this is an average value as the thickness of Earth's magnetized layer is actually varying, with the largest contrast present at the boundary between oceans and continents. In regions where the magnetized layer is thicker (thinner) than the average value considered here, the intensity of the estimated visible magnetization is an overestimation (underestimation) of the intensity of the actual visible magnetization. Moreover, due to this assumption,

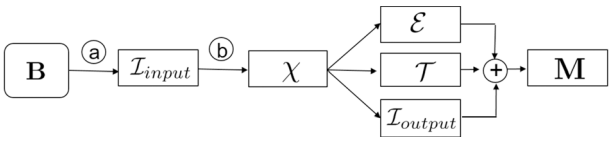

Figure 1. A schematic representation of our algorithm. The curved block represents input, in particular, **B** stands for the input lithospheric field model. All rectangular blocks represent output, in particular, $\mathcal{I}_{\text{input}}$ stands for the visible magnetization model obtained through the conversion formula of equation (4); χ for the output susceptibility model, $\mathcal{I}_{\text{output}}$, $\mathcal{E}$, and $\mathcal{T}$ for the visible, hidden poloidal, and hidden toroidal parts of the magnetization, respectively, obtained by means of the output susceptibility model; and **M** for the total magnetization. The circles represent incorporated assumptions. In particular, a stands for the assumed thickness of the magnetized layer, in which the magnetization varies only laterally and b for the a priori susceptibility model, the dipolar inducing field, and the assumption of induced magnetization. For details see section 3.

magnetic field signal due to gradients in the thickness of the magnetized layer is represented in our results as gradients in the magnetization intensity.

3.2. From the Visible Magnetization to the Magnetic Susceptibility

If the magnetization is induced by a magnetic field of internal origin $\mathbf{B}_{\text{inducing}}$ and the magnetic susceptibility χ is isotropic, then the magnetization writes

$$\mathbf{M}_{\text{induced}}(\mathbf{r}) = \frac{\chi(\mathbf{r})}{\mu_0}\mathbf{B}_{\text{inducing}}(\mathbf{r}), \tag{5}$$

with **r** the position vector of the magnetized point. Expressing now both the susceptibility distribution and the inducing magnetic field in terms of SH, we obtain

$$g^m_{I,l} = \frac{1}{4\pi\mu_0}\sum_{\tilde{l},\tilde{m}}\alpha^{\tilde{m}}_{\tilde{l}}\sum_{l',m'}g^{m'}_{l'}\left(\frac{R}{r}\right)^{l'+2}G^{\tilde{m},m',m}_{\tilde{l},l',l}A_{\tilde{l},l',l}, \tag{6}$$

where $A_{\tilde{l},l',l} = -\frac{1}{2}\sqrt{\frac{2l+1}{l}}\left\{l'(l'+1)+l(l+1)-\tilde{l}(\tilde{l}+1)-2l(l'+1)\right\}$, $\alpha^{\tilde{m}}_{\tilde{l}}$ are the SH coefficients of the susceptibility, $g^{m'}_{l'}$ are the SH coefficients of the inducing magnetic field, and $G^{\tilde{m},m',m}_{\tilde{l},l',l}$ are the Gaunt integrals: $G^{\tilde{m},m',m}_{\tilde{l},l',l} = \int Y^{\tilde{m}}_{\tilde{l}}Y^{m'}_{l'}Y^{m}_{l}\mathrm{d}\Omega$.

Given the SH coefficients of an inducing magnetic field, equation (6), allows deriving the SH coefficients of the susceptibility from the SH coefficients of the visible magnetization. Here we considered a dipolar inducing field, defined by the SH coefficients of degree 1 of the GFZ Reference Internal Magnetic Model (GRIMM) core magnetic field model at epoch 2005.5 (Lesur et al., 2008). We note that Earth's core magnetic field is dominantly dipolar, with the dipolar component contributing by more than 90% to the field's energy at the Earth's surface (e.g., Lanza & Meloni, 2006).

The lithospheric magnetic field model and the resulted visible magnetization model have both a limited spatial resolution characterized by a maximum SH degree l_{max}, here equal to 200. Assuming a dipolar inducing field, the exclusion rules of the Gaunt integrals impose that the maximum SH degree of the susceptibility distribution contributing to equation (6) is $\tilde{l}_{\text{max}} = l_{\text{max}}+1$. Therefore, the susceptibility model has $(l_{\text{max}}+2)^2$ degrees of freedom, of which $2l_{\text{max}}+4$ remains unconstrained by the visible magnetization model, including the case of a layer of constant susceptibility. These unconstrained parts of the susceptibility distribution have been described by Maus and Haak (2003), who called them annihilators. However, contrary to their use of this term to describe interchangeably distributions of magnetization or susceptibility that give rise to no observable magnetic field, we use it here exclusively for the part of the susceptibility that gives rise to no observable magnetic field. For susceptibility annihilators to be estimated, a priori information is required. Here we constrain the annihilators using the VIS model by Hemant and Maus (2005), solving, therefore, a regularized inverse problem (see the supporting information for details).

The obtained susceptibility model is shown in supporting information Figure S1. Due to our assumption of a magnetized layer of constant thickness, high magnetization values indicate locations with high magnetic susceptibility and/or thick magnetized crust; we do not distinguish between these two possible sources of magnetization. In this sense, the output susceptibility model is an equivalent susceptibility model.

3.3. From the Magnetic Susceptibility to the Hidden Magnetization

Once the magnetic susceptibility is obtained, simple forward calculations give the hidden part of the magnetization. In the same way as for equation (6), we obtain the expressions that relate the vector SH coefficients of the poloidal and toroidal parts of the hidden magnetization, $\mathcal{E}$ and $\mathcal{T}$, to the SH coefficients of the susceptibility and of the inducing magnetic field:

$$g^m_{\mathcal{E},l} = \frac{1}{4\pi\mu_0}\sum_{\tilde{l},\tilde{m}}\alpha^{\tilde{m}}_{\tilde{l}}\sum_{l',m'}g^{m'}_{l'}\left(\frac{R}{r}\right)^{l'+2}G^{\tilde{m},m',m}_{\tilde{l},l',l}B_{\tilde{l},l',l}, \tag{7}$$

and

$$g^m_{\mathcal{T},l} = \frac{1}{4\pi\mu_0}\sum_{\tilde{l},\tilde{m}}\alpha^{\tilde{m}}_{\tilde{l}}\sum_{l',m'}g^{m'}_{l'}\left(\frac{R}{r}\right)^{l'+2}E^{\tilde{l},l',l}_{\tilde{m},m',m}\frac{2l+1}{\sqrt{l(l+1)}}, \tag{8}$$

with $B_{\tilde{l},l',l} = -\frac{1}{2}\sqrt{\frac{2l+1}{l+1}}\left\{l'(l'+1)+l(l+1)-\tilde{l}(\tilde{l}+1)+2(l+1)(l'+1)\right\}$ and $E^{\tilde{l},l',l}_{\tilde{m},m',m}$ the Elsasser integrals

$$E^{\tilde{l},l',l}_{\tilde{m},m',m} = -r^2\int Y^{\tilde{m}}_{\tilde{l}}\left(\nabla_H Y^{m'}_{l'}\right)\left[\nabla_H\times\left(\hat{r}Y^m_l\right)\right]\mathrm{d}\Omega.$$

The poloidal and toroidal parts of the hidden magnetization are shown in supporting information Figures S2 and S3, respectively, and their sum in supporting information Figure S4. Supporting information Figure S5 shows the output visible magnetization, obtained through forward calculation of equation (6) ($\mathcal{I}_{\text{output}}$ in Figure 1).

According to equations (6)–(8), the largest part of a given magnetic susceptibility distribution gives rise to both a visible and a hidden magnetization. The susceptibility annihilators are only responsible for a small fraction of the hidden magnetization.

4. Results

4.1. The Magnetization

The sum of the visible and hidden parts, that is, the entire magnetization, is shown in Figure 2. Integrating the square of the intensity of the different parts (Gubbins et al., 2011), we find that the visible magnetization accounts for only 38% of the total magnetization and the hidden magnetization for the remaining 62%. The output visible magnetization differs not only in intensity from the total magnetization but also in direction (see supporting information Figure S6). Since the total magnetization is aligned with the inducing magnetic field, this result shows that the visible part of the magnetization does not preserve the information of the inducing field direction (as demonstrated by Vervelidou, Lesur, Morschhauser, et al. 2017).

Figure 3 shows the intensity of the input lithospheric field model (a), the output visible magnetization model (b), the hidden magnetization (c), and the total magnetization (d). According to this figure, the hidden magnetization is everywhere at least as strong as the visible magnetization. At middle and high latitudes, the visible and hidden magnetization structures have similar intensity and shape (e.g., over North America, Europe, and Australia; marked with yellow boxes on all four maps). In low latitudes, magnetization is strongly dominated by its hidden part (e.g., over southern America, central Africa at the location of the renown Bangui magnetic anomaly, and India; marked with maroon boxes on all four maps). There, both the shape and the intensity of the hidden magnetization differ from the visible one. For example, we notice a strongly magnetized structure along the Chagos-Laccadive Ridge in the Indian Ocean, which is absent in the visible magnetization map. Although this structure appears due to our a priori susceptibility map, and in particular due to the high susceptibility assigned by Hemant and Maus (2005) to oceanic plateaus, our results demonstrate that such a structure would generate no magnetic field signal. Similarly, the total magnetization underlying the Bangui magnetic anomaly has a much more elongated structure than its visible magnetization component. Both a geological (e.g., Ouabego et al., 2013) and an impact origin have been suggested for this prominent magnetic anomaly (e.g., Girdler et al., 1992), and it has been explained both in terms of important remanent magnetization and induced magnetization. In particular, Hemant and Maus (2005) constructed their VIS model in a way that this magnetic anomaly is reproduced in terms of induced magnetization, invoking basaltic composition for parts of the lower crust and upper crust of the region. Our results, making use of their VIS model, reproduce most of the Bangui anomaly (note the residuals between the input and output lithospheric field models shown in supporting information Figure S8) on the basis of induced magnetization, which is mathematically possible for any magnetic field anomaly. The contribution of our study in respect to this anomaly concerns the shape of the underlying magnetization and in particular the delineation of its arched geometry. This geometry follows the pattern of the Archean provinces present in this region but could also be suggestive of a portion of a crater ring. As for the hidden magnetization over southern America, we observe that this is again mainly concentrated over the Archean portions of the regional crust, located around the Amazon river. We note that our input lithospheric field model is based on the 2016 version of the WDMAM, which does not include the latest available Brazilian aeromagnetic survey. This has since been made available and incorporated into the WDMAM.

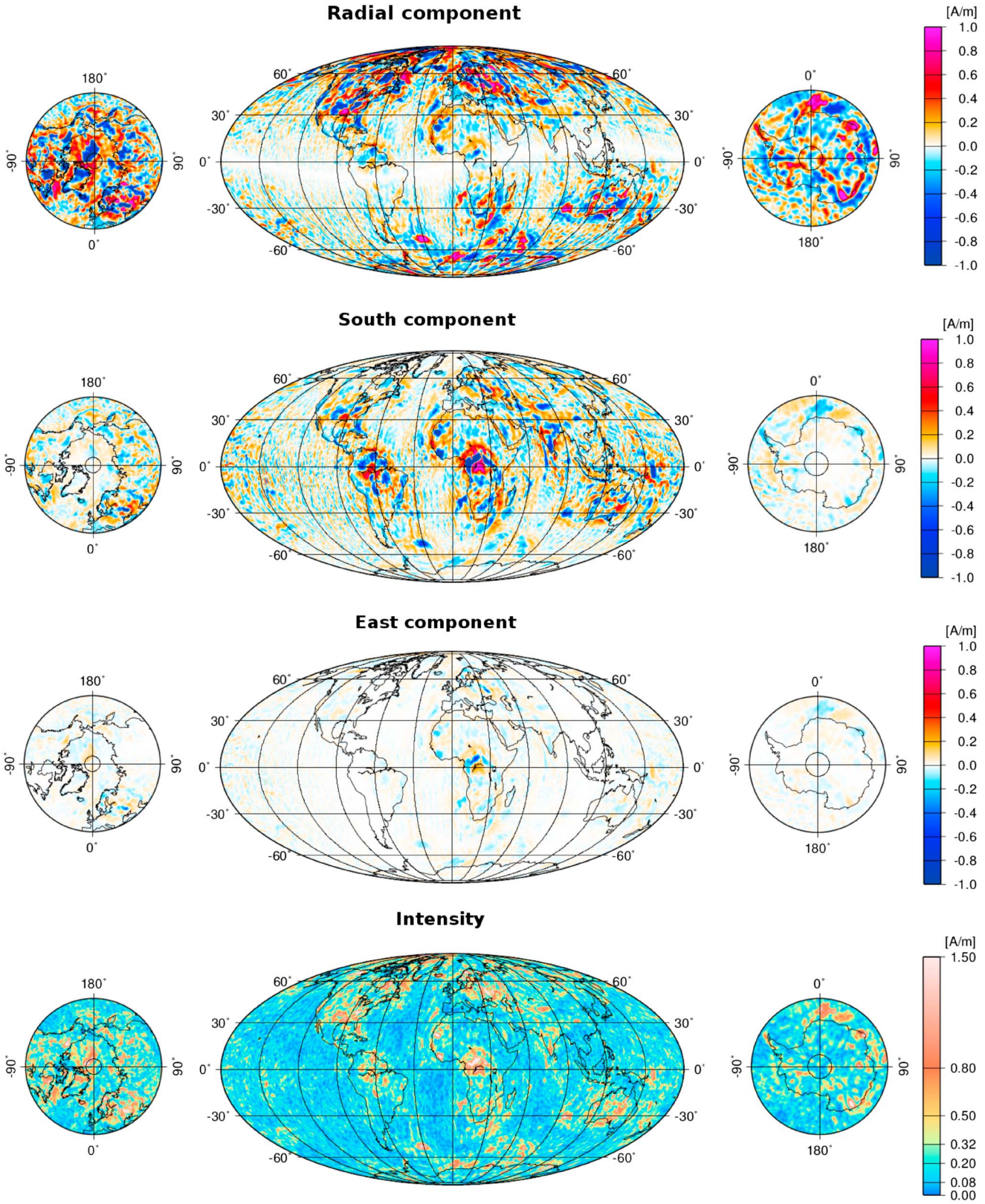

Figure 2. The total magnetization obtained in this study. The three vector components and the intensity are shown. The left column shows an orthographic projection of the north polar cap, down to 60°N, the middle column shows a Mollweide projection of all latitudes, and the right column shows an orthographic projection of the south polar cap, up to 60°S.

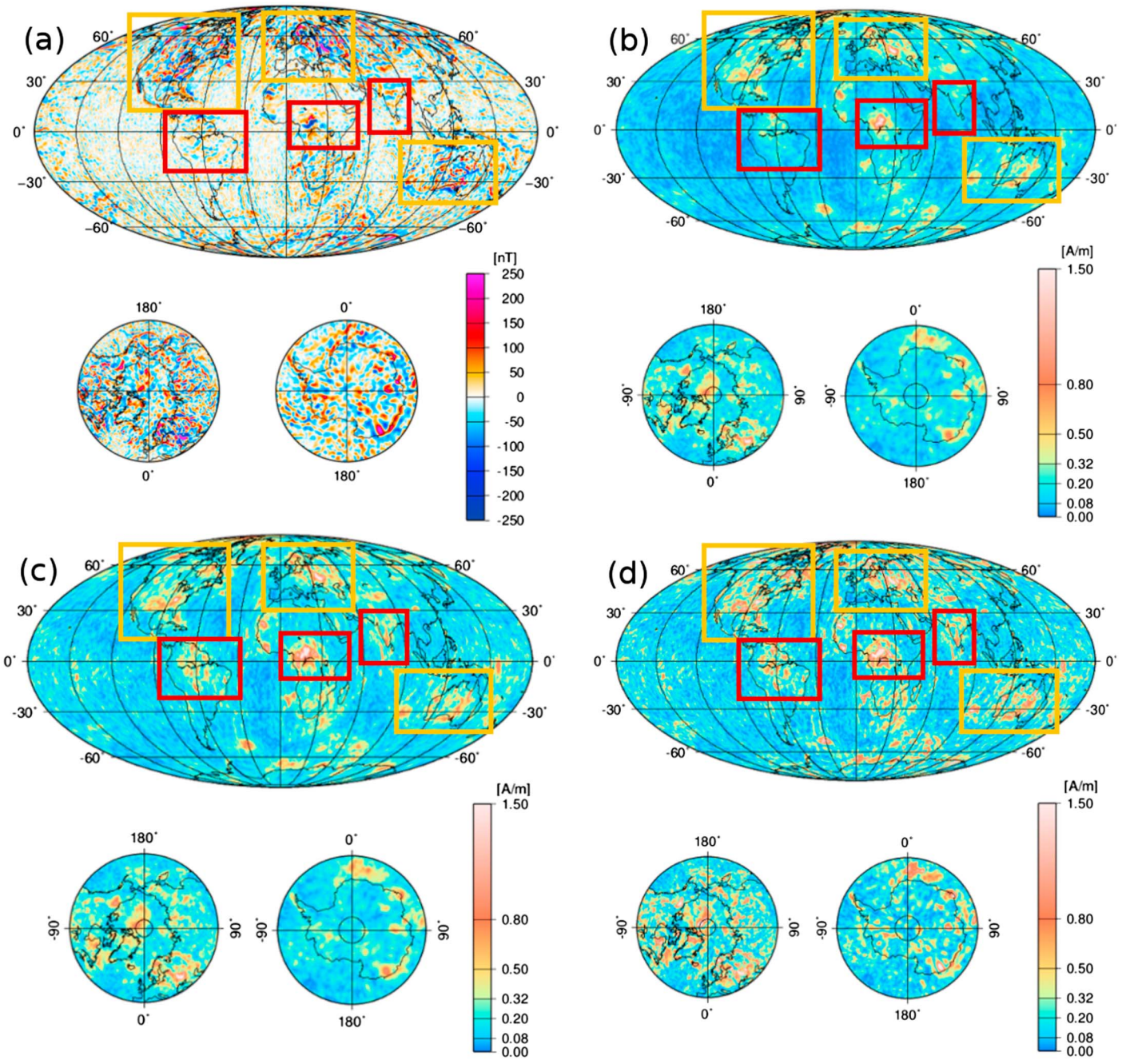

Figure 3. The contribution of hidden magnetization. The intensity of (a) the input lithospheric field model, (b) the output visible magnetization model, (c) the hidden magnetization model, and (d) the total magnetization model. Yellow boxes denote areas where the visible and the hidden magnetization are similar in shape and strength and, therefore, contribute equally to the total magnetization. Maroon boxes denote areas where the hidden magnetization prevails over the visible one and is, therefore, the component that mainly shapes the total magnetization.

4.2. The Role of the A Priori Information

To distinguish between the contribution of the lithospheric magnetic field model and the a priori susceptibility model to the total magnetization, we solved a second inverse problem. This time we inverted for the SH coefficients of the susceptibility distribution, using equation (6), without the use of a priori information. For this, we eliminated the unconstrained part of the inversion by setting it to zero (winnowing technique; see, e.g., Gubbins, 2004). The obtained hidden magnetization is shown in Figure 4a. The differences in respect to the hidden magnetization obtained using the regularized inverse problem are shown in Figure 4b. They exhibit oscillations that are not apparent in Figure 3c thanks to the information introduced through the a priori

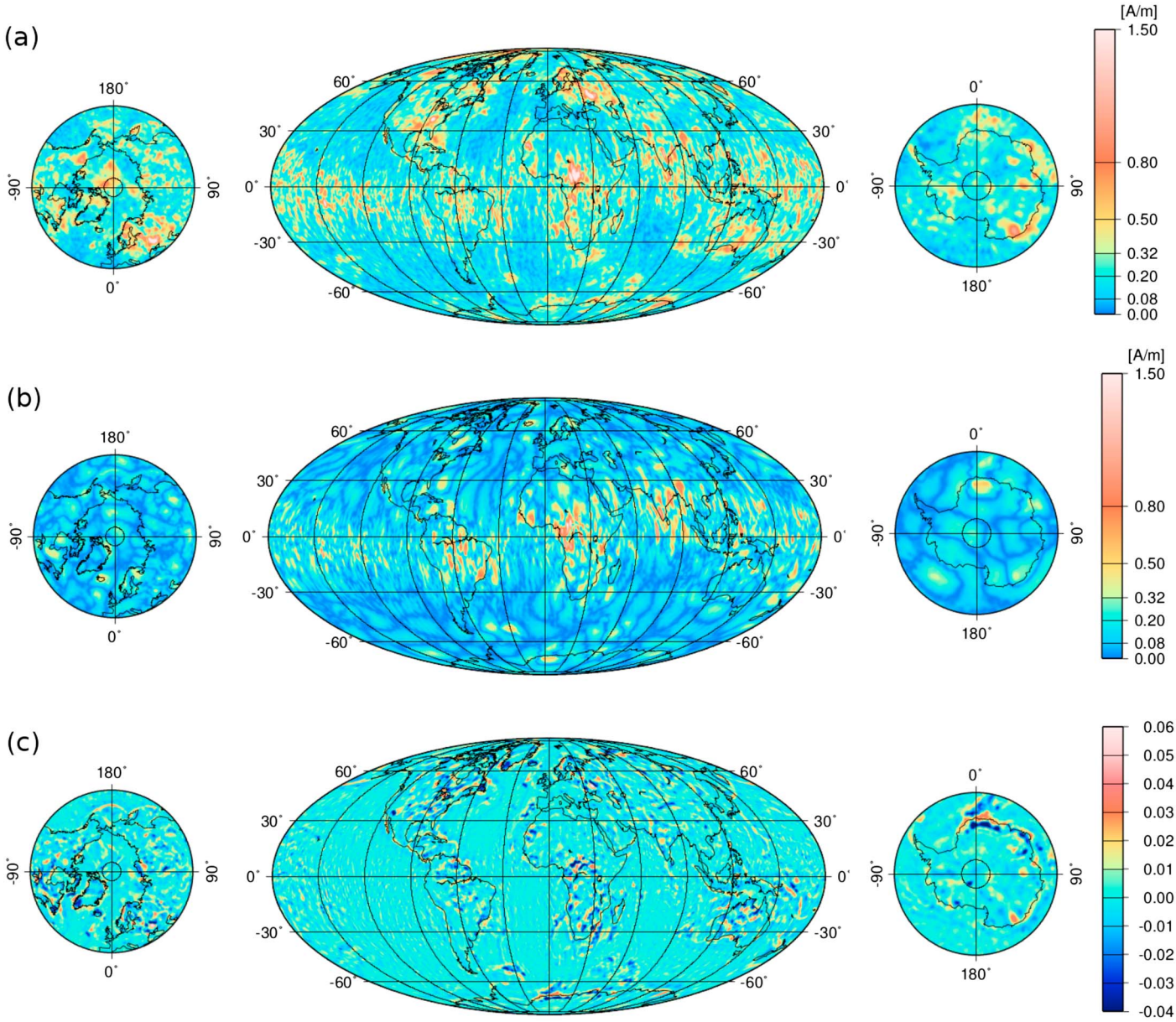

Figure 4. The contribution of the a priori information. (a) The hidden magnetization retrieved from the magnetic field model, without the use of a priori information. (b) The difference between panel (a) and the hidden magnetization obtained through the regularized inverse problem (shown in Figure 3c). (c) The residuals between the output and input susceptibility models.

susceptibility model. These oscillations are concentrated along the magnetic equator in agreement with our theoretical calculations (see the supporting information). It is, therefore, precisely along the magnetic equator, where the inducing magnetic field is purely horizontal, that we expect the most substantial changes given a different a priori susceptibility model. In this respect, the hidden magnetization component over southern America, the Bangui magnetic anomaly, and India is strongly conditioned by our a priori.

To infer the reliability of the a priori model at low latitudes, where the magnetic field model is an inadequate source of information, we investigate to which degree our a priori is compatible with the input magnetic field model at middle and high latitudes. For this, we show in Figure 4c the residuals between the a priori susceptibility model and the susceptibility model obtained after solving the regularized inverse problem. According to this figure, the residuals are uniformly distributed over all latitudes. We do not observe larger residuals over middle and high latitudes, where the primary source of information is the magnetic field model, than over low latitudes, where the primary source of information is the a priori model itself. This observation gives us

some confidence that the a priori susceptibility model is reliable also over low latitudes and that indeed the magnetization there is dominated by its hidden component.

The role of the a priori is crucial for recovering the magnetization of SH degrees 0–15. In the absence of lithospheric magnetic field data over this bandwidth, the only source of information is then the a priori susceptibility model. However, since we are interested in the information about the magnetization that can be retrieved from magnetic field data, we exclude this part of the a priori susceptibility model from our inversion (see the supporting information for details).

5. Conclusions

Magnetization is a quantity directly related to a number of properties of the uppermost lithosphere like composition, temperature, hydrothermal activity, and crustal thickness. As such it can be a valuable source of information for lithospheric studies. However, retrieving the magnetization distribution associated with a given magnetic field set of measurements in a unique way has been a long-standing open question in geophysics that has severely restricted the use of magnetic data for probing solid Earth's upper layers. Decomposing the magnetization into three parts, from which only the one contributes to the observed magnetic field and is therefore directly recoverable from magnetic field measurements, constituted an important step forward (Baratchart et al., 2012; Gerhards, 2015, 2019; Gubbins et al., 2011).

Building on this formalism, we demonstrated here that for a magnetization of purely induced origin, these three parts, namely, the visible magnetization, the hidden poloidal magnetization, and the hidden toroidal magnetization, are linked to each other through the susceptibility distribution and the inducing magnetic field. This link enables us to recover the largest part of the hidden magnetization through the knowledge of the visible magnetization. The part of the hidden magnetization that remains inaccessible from magnetic data is due to a small, well-understood part of the underlying susceptibility, mainly lying around the magnetic equator, which gives rise only to hidden magnetization. Recovering this part requires input from independent, a priori information. Once the entire susceptibility is recovered, so is the entire induced magnetization.

We applied our methodology on Earth, and the results obtained reveal that the hidden magnetization accounts for 62% of Earth's magnetization. We show that at middle and high latitudes, where the main source of information is the input lithospheric magnetic field model, Earth's hidden magnetization is very similar to the visible magnetization, both in intensity and in shape. At low latitudes, the magnetization relies heavily on the a priori susceptibility model used in the inversion scheme. There, our results show that several structures of the a priori susceptibility model give rise only to hidden magnetization. We conclude that recovering the entire magnetization allows new magnetized structures to become apparent and other, known ones, to become more accurately delineated. In both cases a more accurate link to the underlying Earth processes becomes possible.

Our study fills in one of the missing pieces in our understanding of Earth's lithospheric magnetization. Moreover, it opens new avenues for lithospheric studies by setting the framework for a joint analysis of magnetic, geological, and other geophysical data. Following this path should facilitate interdisciplinary studies and enhance our understanding of Earth's interior. Extending our formalism to regional and local scales, allowing to account for a magnetized layer of variable thickness, and separating induced from remanent magnetization are direct perspectives of our study. They will allow for a more detailed look into properties of the solid Earth and also its dynamics, as reflected upon the remanent component of Earth's magnetization. A similar methodology can be applied to the study of other terrestrial bodies with magnetized crust, like Mars and the Moon, allowing us to decipher some of the long-standing open questions related to their formation and evolution.

Acknowledgments
We wish to thank Michael Purucker and an anonymous reviewer for valuable comments that helped us improve the manuscript. F. V. was funded by the Deutsche Forschungsgemeinschaft (German Research Foundation, DFG), within the Priority Program 1788 *Dynamic Earth* under the grant LE2477/7-1. V. L. was partly supported by the *Centre National des Etudes Spatiales (CNES)* within the context of the project: *Travaux préparatoires et exploitation de la mission Swarm*. We thank ESA for free access to Swarm DISC products and the WDMAM Task Force for free access to WDMAM products (https://doi.org10.18715/wdmam.2.0). The input lithospheric field model up to SH degree 90 is freely available at ftp://swarm-diss.eo.esa.int (for details see https://earth.esa.int/web/guest/content/-/article/swarm-data-access) and beyond SH degree 90 from http://wdmam.org. We thank Kumar Hemant Singh for providing us with the VIS model by Hemant and Maus (2005).

References

Arkani-Hamed, J., & Strangway, D. W. (1985). Lateral variations of apparent magnetic susceptibility of lithosphere deduced from Magsat data. *Journal of Geophysical Research*, *90*, 2655–2664.

Baratchart, L., Hardin, D. P., Lima, E. A., Saff, E. B., & Weiss, B. P. (2012). Characterizing kernels of operators related to thin-plate magnetizations via generalizations of Hodge decompositions. *Inverse Problems*, *29*(1), 15004.

Besse, J., & Courtillot, V. (2002). Apparent and true polar wander and the geometry of the geomagnetic field over the last 200 Myr. *Journal of Geophysical Research*, *107*(B11), 2300. https://doi.org/10.1029/2000JB000050

Blakely, R. J. (1996). *Potential theory in gravity and magnetic applications*. California: Cambridge University Press.

Dyment, J., Choi, Y., Hamoudi, M., Lesur, V., & Thébault, E. (2015). Global equivalent magnetization of the oceanic lithosphere. *Earth and Planetary Science Letters*, *430*, 54–65.

Ferré, E. C., Friedman, S. A., Martín-Hernández, F., Feinberg, J. M., Till, J. L., Ionov, D. A., & Conder, J. A. (2014). Eight good reasons why the uppermost mantle could be magnetic. *Tectonophysics*, *624*, 3–14.
Fox Maule, C., Purucker, M. E., Olsen, N., & Mosegaard, K. (2005). Heat flux anomalies in Antarctica revealed by satellite magnetic data. *Science*, *309*, 464–467.
Friis-Christensen, E., Lühr, H., & Hulot, G. (2006). Swarm: A constellation to study the Earth's magnetic field. *Earth Planets Space*, *58*, 351–358.
Gerhards, C. (2015). On the unique reconstruction of induced spherical magnetizations. *Inverse Problems*, *32(1)*, 15002.
Gerhards, C. (2019). On the reconstruction of inducing dipole directions and susceptibilities from knowledge of the magnetic field on a sphere. *Inverse Problems in Science and Engineering*, *27*(1), 37–60. https://doi.org/10.1080/17415977.2018.1438426
Girdler, R. W., Taylor, P. T., & Frawley, J. J. (1992). A possible impact origin for the Bangui magnetic anomaly (Central Africa). *Tectonophysics*, *212*, 45–58.
Gubbins, D. (2004). *Time series analysis and inverse theory for geophysicists*. Cambridge, UK: Cambridge University Press.
Gubbins, D., Ivers, D., Masterton, S. M., & Winch, D. E. (2011). Analysis of lithospheric magnetization in vector spherical harmonics. *Geophysical Journal International*, *187*, 99–117.
Hemant, K., & Maus, S. (2005). Geological modeling of the new CHAMP magnetic anomaly maps using a Geographical Information System (GIS) technique. *Journal of Geophysical research*, *110*, B12103. https://doi.org/10.1029/2005JB003837
Jackson, A., Winch, D., & Lesur, V. (1999). Geomagnetic effects of the Earth's ellipticity. *Geophysical Journal International*, *138*(1), 285–289.
Khorhonen, J. K., Fairhead, J. D, Hamoudi, M., Hemant, K., Lesur, V., Mandea, M., et al. (2007). Magnetic anomaly map of the world-carte des anomalies magnétiques du monde. Commission for the Geological Map of the World. (Scale: 1:50,000,000, 1st edition, Paris, France).
Lanza, R., & Meloni, A. (2006). *The Earth's magnetism*. Heidelberg: Springer-Verlag Berlin Heidelberg.
Lesur, V., Hamoudi, M., Choi, Y., Dyment, J., & Thébault, E. (2016). Building the second version of the World Digital Magnetic Anomaly Map (WDMAM). *Earth, Planets and Space*, *68*(1), 27.
Lesur, V., & Jackson, A. (2000). Exact solutions for internally induced magnetization in a shell. *Geophysical Journal International*, *140*(2), 453–459.
Lesur, V., Wardinski, I., Rother, M., & Mandea, M. (2008). GRIMM—The GFZ Reference Internal Magnetic Model based on vector satellite and observatory data. *Geophysical Journal International*, *173*, 382–394.
Masterton, S. M., Gubbins, D., Müller, R. D., & Singh, K. H. (2013). Forward modelling of oceanic lithospheric magnetization. *Geophysical Journal International*, *192*, 951–962.
Maus, S., & Haak, V. (2003). Magnetic field annihilators: Invisible magnetization at the magnetic equator. *Geophysical Journal International*, *155*(2), 509–513.
Maus, S., Rother, M., Hemant, K., Stolle, C., Lühr, H., Kuvshinov, A., & Olsen, N. (2006). Earth's lithospheric magnetic field determined to Spherical Harmonic degree 90 from CHAMP satellite measurements. *Geophysical Journal International*, *164*, 319–330.
Ouabego, M., Quesnel, Y., Rochette, P., Demory, F., Fozing, E. M., Njanko, T., et al. (2013). Rock magnetic investigation of possible sources of the Bangui magnetic anomaly. *Physics of the Earth and Planetary Interiors*, *224*, 11–20.
Parker, R. L. (2003). Ideal bodies for Mars magnetics. *Journal of Geophysical Research*, *108*(E1), 5006. https://doi.org/10.1029/2001JE00760
Purucker, M. E., Langel, R. A., Rajaram, M., & Raymond, C. (1998). Global magnetization models with a priori information. *Journal of Geophysical Research*, *103*(B2), 2563–2584.
Quesnel, Y., Weckmann, U., Ritter, O., Stankiewicz, J., Lesur, V., Mandea, M., et al. (2009). Simple models for the Beattie Magnetic Anomaly in South Africa. *Tectonophysics*, *478*(1-2), 111–118.
Runcorn, S. K. (1975). An ancient lunar magnetic dipole field. *Nature*, *253*, 701–703.
Thébault, E., Purucker, M., Whaler, K. A., Langlais, B., & Sabaka, T. J. (2010). The magnetic field of the Earth's lithosphere. *Space Science Reviews*, *155*, 95–127.
Thébault, E., & Vervelidou, F. (2015). A statistical spatial power spectrum of the Earth's lithospheric magnetic field. *Geophysical Journal International*, *201*, 605–620.
Thébault, E., Vigneron, P., Langlais, B., & Hulot, G. (2016). A Swarm lithospheric magnetic field model to SH degree 80. *Earth, Planets and Space*, *68*, 126.
Vervelidou, F., Lesur, V., Grott, M., Morschhauser, A., & Lillis, R. J. (2017). Constraining the date of the Martian dynamo shutdown by means of crater magnetization signatures. *Geophysical Research: Planets*, *122*, 2294–2311. https://doi.org/10.1002/2017JE005410
Vervelidou, F., Lesur, V., Morschhauser, A., Grtt, M., & Thomas, P. (2017). On the accuracy of paleopole estimations from magnetic field measurements. *Geophysical Journal International*, *211*, 1669–1678.
Vervelidou, F., & Thébault, E. (2015). Global maps of the magnetic thickness and magnetization of the Earth's lithosphere. *Earth, Planets and Space*, *67*, 173.
Vine, F. J., & Matthews, D. H. (1963). Magnetic anomalies over oceanic ridges. *Nature*, *199*(4897), 947–949.
Wasilewski, P. J., Thomas, H. H., & Mayhew, M. A. (1979). The Moho as a magnetic boundary. *Geophysical Research Letters*, *6*(7), 541–544.
Whaler, K. A., & Langel, R. A. (1996). Minimal crustal magnetizations from satellite data. *Physics of the Earth and Planetary Interiors*, *98*, 303–319.